The Role of Tropical Cyclones in the Formation of Tropical Upper-Tropospheric Troughs

ROSANA NIETO FERREIRA

Universities Space Research Association, NASA/GSFC Laboratory for Atmospheres, Greenbelt, Maryland

WAYNE H. SCHUBERT

Department of Atmospheric Science, Colorado State University, Fort Collins, Colorado

(Manuscript received 21 March 1997, in final form 15 December 1998)

ABSTRACT

Tropical upper-tropospheric troughs (TUTTs), also known as midoceanic troughs, are elongated troughs that appear in summer monthly averaged maps of the upper-tropospheric flow over the oceans. The transient part of these climatological features is composed of TUTT cells and their origin is the subject of this study.

TUTT cells often occur to the east of tropical cyclones. A nonlinear shallow water model on the sphere was used in a simplified study of the interactions between tropical cyclones and the circumpolar vortex. Based on the results of these simulations and keeping in mind their limitations, it is proposed that dispersion of short Rossby wave energy is a possible mechanism to explain the formation of TUTT cells to the east of tropical cyclones. The model simulations suggest that two types of TUTT cells may form to the east of tropical cyclones. When embedded in cyclonic or weak anticyclonic shear, the trough to the east of the tropical cyclone may broaden, resulting in the formation of an intense TUTT cell that has a strong signature in the wind and mass fields. In the presence of stronger anticyclonic shear, the trough to the east of the tropical cyclone may become a thin and elongated TUTT cell that has a comparatively negligible signature in the mass and flow fields. Moreover, the model simulations indicate that the mode of evolution of TUTT cells that form to the east of a tropical cyclone is strongly dependent on the intensity and relative location of midlatitude waves.

Wave–mean flow interaction calculations indicated that tropical cyclones produced a westerly acceleration of the mean zonal flow in the latitudinal band through which they move and an easterly acceleration elsewhere. These calculations also indicated that broadening TUTT cells may cause an easterly acceleration of the zonal mean flow.

1. Introduction

Tropical upper-tropospheric troughs (TUTTs), also known as midoceanic troughs, are elongated troughs that appear in summer monthly averaged maps of the upper-tropospheric flow over the oceans (Sadler 1975). These climatological features can be decomposed into stationary and transient eddy parts. The stationary part is believed to be maintained by the intertropical convergence zone (ITCZ) convection over the Americas (Silva Dias et al. 1983), Asia, Australia, and the west Pacific warm pool region (e.g., Webster 1972; Colton 1973; Hoskins and Rodwell 1995). The transient part is composed of TUTT cells and their origin is the main subject of this study.

Previous studies have found that TUTT cells can cause changes in the development and movement of tropical cyclones. Depending on its position relative to a tropical cyclone, a TUTT cell can cause a decrease in intensity or inhibition of genesis by increasing the vertical wind shear in which the tropical cyclone is embedded (e.g., Gray 1968). On the other hand, when the vertical wind shear does not exceed a certain threshold, TUTT cells may aid in the genesis and intensification of tropical cyclones (e.g., Pfeffer and Challa 1992; Montgomery and Farrell 1993; Molinari et al. 1995). Moreover, since the cyclonic circulation associated with TUTT cells can extend to the middle and even lower troposphere, they sometimes influence the mean steering currents in which tropical cyclones are embedded, possibly contributing to recurvature (e.g., Hodanish and Gray 1993). In addition, TUTT cells may play a role in troposphere–stratosphere exchange (Holton et al. 1995; Price and Vaughan 1993) and in modulating the mean meridional circulation of the atmosphere.

Observational studies (e.g., Kelley and Mock 1982; Whitfield and Lyons 1992; Price and Vaughan 1992) have found that TUTT cells are cold core cyclones con-

Corresponding author address: Dr. Rosana Nieto Ferreira, NASA/GSFC, Mailcode 913.0, Greenbelt, MD 20771.
E-mail: ferreira@janus.gsfc.nasa.gov

fined to the layer between 100 and 700 mb, whose typical horizontal scale is of the order of several hundred kilometers. The coldest temperature anomaly in a TUTT cell occurs near 300 mb with the maximum cyclonic circulation near 200 mb. They typically last for less than five days but may, in some cases, persist for nearly two weeks. In the Northern Hemisphere, these systems often move to the west-southwest and are characterized by subsidence and minimum cloudiness in their northwest quadrant and ascent and maximum cloudiness in their southeast (SE) quadrant.

Yet few studies have addressed the origin of TUTT cells, and issues such as their frequency of occurrence and modes of formation are not well known. Observations suggest that an important source of potential vorticity (PV) for TUTT cells is the large reservoir of high PV in the circumpolar vortex (Whitfield and Lyons 1992). One of the mechanisms for the extrusion of pockets of high PV air from the circumpolar vortex is a type of baroclinic wave development in which the midlatitude trough penetrates into lower latitudes becoming embedded in anticyclonic shear. In this environment, the midlatitude trough becomes increasingly elongated, thin, and northeast–southwest (NE-SW) oriented (in the Northern Hemisphere) as it is advected westward and equatorward (Thorncroft et al. 1993). Such thinning midlatitude troughs may subsequently either roll up into one large cyclone or break down into several smaller cyclones through barotropic instability.[1] When the resulting cyclones become cut off from the circumpolar vortex and wander into the Tropics during the summer months they are called TUTT cells. Incidentally, the formation of cutoff lows by this mechanism also occurs during the winter (e.g., Appenzeller et al. 1996; Price and Vaughan 1993). This process is dynamically analogous to Rossby wave breaking in the stratospheric polar vortex (e.g., McIntyre and Palmer 1984).

In the Pacific Ocean, another mode of TUTT cell genesis is common, namely, shear instability in strongly sheared regions on the edge of the circumpolar vortex (Kelley and Mock 1982). A numerical study by Colton (1973) suggests that TUTT cells form through barotropic instability of the flow associated with the climatological TUTT, which is in turn produced and kept in place by ITCZ convection.

Another mechanism for the extraction of pockets of high-PV air from the circumpolar vortex involves interactions with nearby tropical cyclones. Both southward advection of high-PV air by the storm's upper-level anticyclone (Habjan and Holland 1995) and dispersion of short Rossby wave energy can lead to the formation of TUTT cells to the east of tropical cyclones. This study focuses on the effects of Rossby wave dispersion, which are simulated with a global shallow water model.

The main limitation of using a shallow water model in this study stems from the inherently different vertical structures of the circumpolar vortex and tropical cyclones. Namely, the circumpolar vortex is a cold core system and, as such, its associated cyclonic winds increase with height to a maximum at the tropopause. On the other hand, a tropical cyclone is a warm core system whose associated cyclonic winds decrease with height from a maximum near the surface. In other words, it could be argued that a TUTT is an upper-tropospheric feature, while the cyclonic tropical cyclone circulation is primarily a lower-tropospheric feature, and therefore their interaction cannot be studied with a barotropic model. However, one may also regard the tropical cyclone as a deep (surface to tropopause) positive anomaly of potential vorticity that excites Rossby wave motion as it moves poleward through a basic-state potential vorticity gradient. We shall show that certain aspects of TUTT structure and evolution can be understood in this simple adiabatic, frictionless, barotropic framework. However, vertical stratification and diabatic effects do play fundamental roles in the evolution of the circumpolar vortex (e.g., Pfeffer 1981; Gallimore and Johnson 1981), midlatitude waves, TUTTs, and tropical cyclones. This barotropic study is but a first step toward understanding the complicated nonlinear patterns of interaction between the circumpolar vortex and a tropical cyclone. Further work on the interaction of tropical cyclones with the circumpolar vortex using a multilayer global model that includes diabetic effects is obviously needed. Indeed, once a TUTT cell has been created through dynamical processes such as the interactions described below in section 3, they can be intensified and maintained by radiational cooling and destroyed by convective heating.

This paper is organized as follows. Section 2 shows an example of the formation and evolution of a TUTT cell in the wake of an Atlantic tropical cyclone using European Centre for Medium-Range Weather Forecasts (ECMWF) analyses and water vapor images. A succinct description of the global nonlinear shallow water model used in this study is given at the begining of section 3. Also presented in section 3 are three simulations of the evolution of the flow when the idealized tropical cyclones are embedded in 1) an environment at rest, 2) a zonally symmetric circumpolar vortex, and 3) an asymmetric circumpolar vortex. Section 4 shows wave–mean flow interaction calculations of the effects of the modeled tropical cyclones upon the zonal mean flow. Section 5 presents conclusions and suggestions for future work.

2. TUTT cells in the wake of Hurricane Felix

In this section, the formation and evolution of TUTT cells in the wake of an Atlantic hurricane will be discussed in the light of *GOES-8* (*Geostationary Opera-*

[1] This is analogous to the formation of frontal waves in midlatitudes (Joly and Thorpe 1990) and to ITCZ breakdown in the Tropics (Nieto Ferreira and Schubert 1997).

tional Environmental Satellite-8) 6.7-μm water vapor imagery and the 2.5° resolution ECMWF analyses. In water vapor images and upper-level isentropic PV plots, TUTT cells appear as dry regions (dark in the water vapor image) of intense cyclonic PV. Given the dryness and large values of PV that are associated with stratospheric air, it is possible that TUTT cells originate as extrusions of midlatitude stratospheric air into the Tropics.

Figure 1 shows a sequence of *GOES-8* water vapor images alongside their nearly simultaneous ECMWF wind and PV fields on the 340-K isentrope for 11–18 August 1995. The *GOES-8* 6.7-μm water vapor channel measures radiation emitted mostly by the atmospheric layer between 200 and 500 mb at a 4-km horizontal resolution.[2] A set of consecutive water vapor images therefore provides a high-resolution view of the upper-tropospheric moisture and horizontal wind fields, being an excellent tool in the study of upper-tropospheric cutoff lows (Appenzeller et al. 1996) of which TUTT cells are a special case. The PV contours have been drawn on the 340-K isentrope using PV units (1 PVU = 10^{-6} m^2 s^{-1} K kg^{-1}). This isentropic level was chosen because as it slants upward from the tropical troposphere to the polar stratosphere, crossing the tropopause somewhere in the midlatitudes; it remains within the 100–400-mb layer. In an adiabatic flow, this means that poleward-moving air ascends and equatorward-moving air descends along isentropic surfaces. In the 340-K isentropic surface, the tropopause is the meandering belt of strong PV gradients in the midlatitudes (Figs. 1a,c,e,g). In the extratropics, the tropopause is usually close to the 2-PVU contour.

During 11–18 August, a TUTT cell formed in the wake of Hurricane Felix and accompanied it in its westward movement across the Atlantic Ocean. Tropical Storm Felix formed on 8 August near 15°N, 33°W. The first signs of the formation of a TUTT cell to the east of Tropical Storm Felix are seen in the 340-K PV fields and water vapor images around 10 August. The storm was upgraded to Hurricane Felix on 11 August near 19°N, 53°W. At that time, the TUTT cell was an elongated tongue of high PV, strong cyclonic winds (Fig. 1a), and dry air (Fig. 1b) that extended into the Tropics, and was located about 26° to the east of the hurricane. By 14 August Hurricane Felix had moved to 30°N, 63°W, and its trailing TUTT cell was located about 20° to its east-southeast. The presence of stratospheric air in the TUTT cell is evidenced by values of PV in excess of 2 PVU (Fig. 1c) and very dry air (Fig. 1d). During 13–18 August, the TUTT cell gradually became more elongated and began to undulate (Figs. 1c,d) and roll up, culminating in its breakdown and formation of two distinct TUTT cells (seen near 25°N, 57°W, and 33°N, 49°W, in Fig. 1f) by 16 August. Being an elongated tongue of high PV, the TUTT cell has a reversed PV gradient in its widthwise direction, indicating that its breakdown may have been caused by barotropic instability. Note the difference in horizontal scale between the two TUTT cells formed by the breakdown of the original TUTT cell. Of the two TUTT cells that resulted from breakdown only the largest one was well resolved in this low-resolution version of the ECMWF analyses. Nevertheless, the collocation of the high-PV values and the dry air in this sequence of maps is remarkable. Such examples of breakdown of PV anomalies are common in nature and occur, for instance, in midlatitude fronts (Joly and Thorpe 1990), the ITCZ (Nieto Ferreira and Schubert 1997), and upper-level cutoff lows (Appenzeller et al. 1996). The largest TUTT cell that resulted from breakdown attained its maximum intensity on 18 August (Figs. 1g,h) and weakened thereafter as it moved southwestward for a few more days. During its approximately 13-day lifetime this TUTT cell accompanied Hurricane Felix in its westward movement across the Atlantic Ocean, interacting with at least four eastward-propagating midlatitude upper-level troughs.

The vertical structure of PV, zonal winds, and potential temperature of this TUTT cell are shown in the meridional cross sections in Fig. 2. On 11 August (Figs. 2a,b) the TUTT cell is evident in the PV cross section as a region of lowered tropopause located between 20° and 30°N. At that time, the signature of this TUTT cell in the zonal wind and potential temperature cross sections was weak. Note, however, that the cyclonic wind shear across the TUTT cell was stronger in the zonal direction than in the meridional direction as indicated in Fig. 1a. The TUTT cell intensifies (Figs. 2c,d) and deepens as it moves westward in the Atlantic Ocean, and by 18 August (Figs. 2e,f) it is a strong cyclonic circulation that occupies the 100–400-mb layer. In the potential temperature cross section (Figs. 2c,e), the TUTT cell was associated with a cold anomaly below and a warm anomaly aloft as seen in the respective upward and downward bowing of the isentropes in that region. The aforementioned wind and potential temperature distributions in the TUTT cell are consistent with the production of balanced flow by an upper-level positive PV anomaly (e.g., Hoskins at al. 1985; Thorpe 1985).

3. Interactions of model tropical cyclones with different mean zonal flows

The global shallow water model on the sphere was used to perform idealized initial value simulations of the interaction of tropical cyclones with their environmental flow. Using spherical coordinates in the horizontal, and denoting the zonal wind by u and the meridional wind by v, the shallow water primitive equations take the form

[2] This vertical interval is biased toward lower pressures in the Tropics.

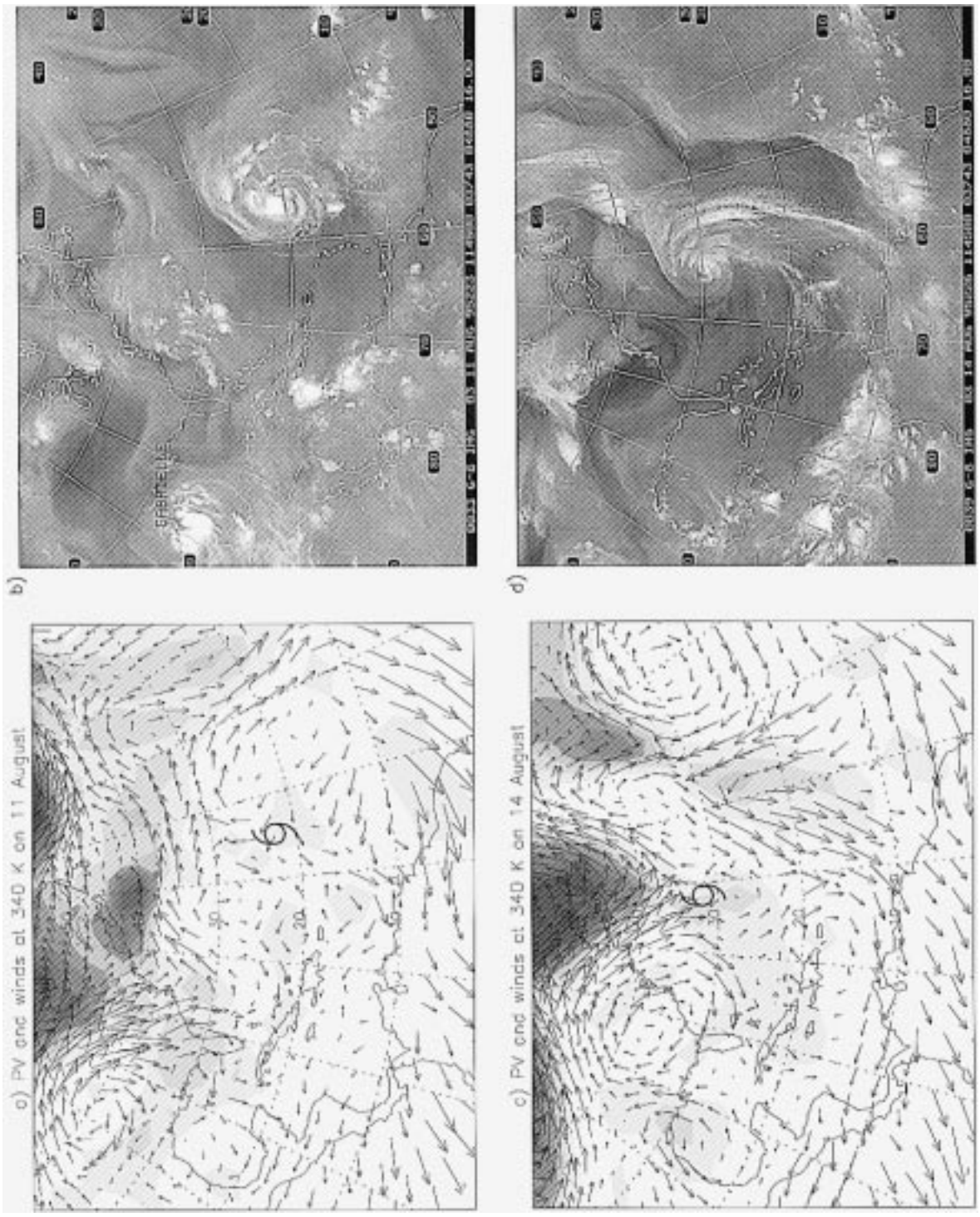

FIG. 1. *GOES-8* water vapor images and nearly simultaneous ECMWF wind and PV fields on the 340-K isentrope for 11–18 Aug 1995. This sequence shows the evolution of a TUTT cell trailing Hurricane Felix. In the PV and wind plots Hurricane Felix's position is indicated by a hurricane symbol.

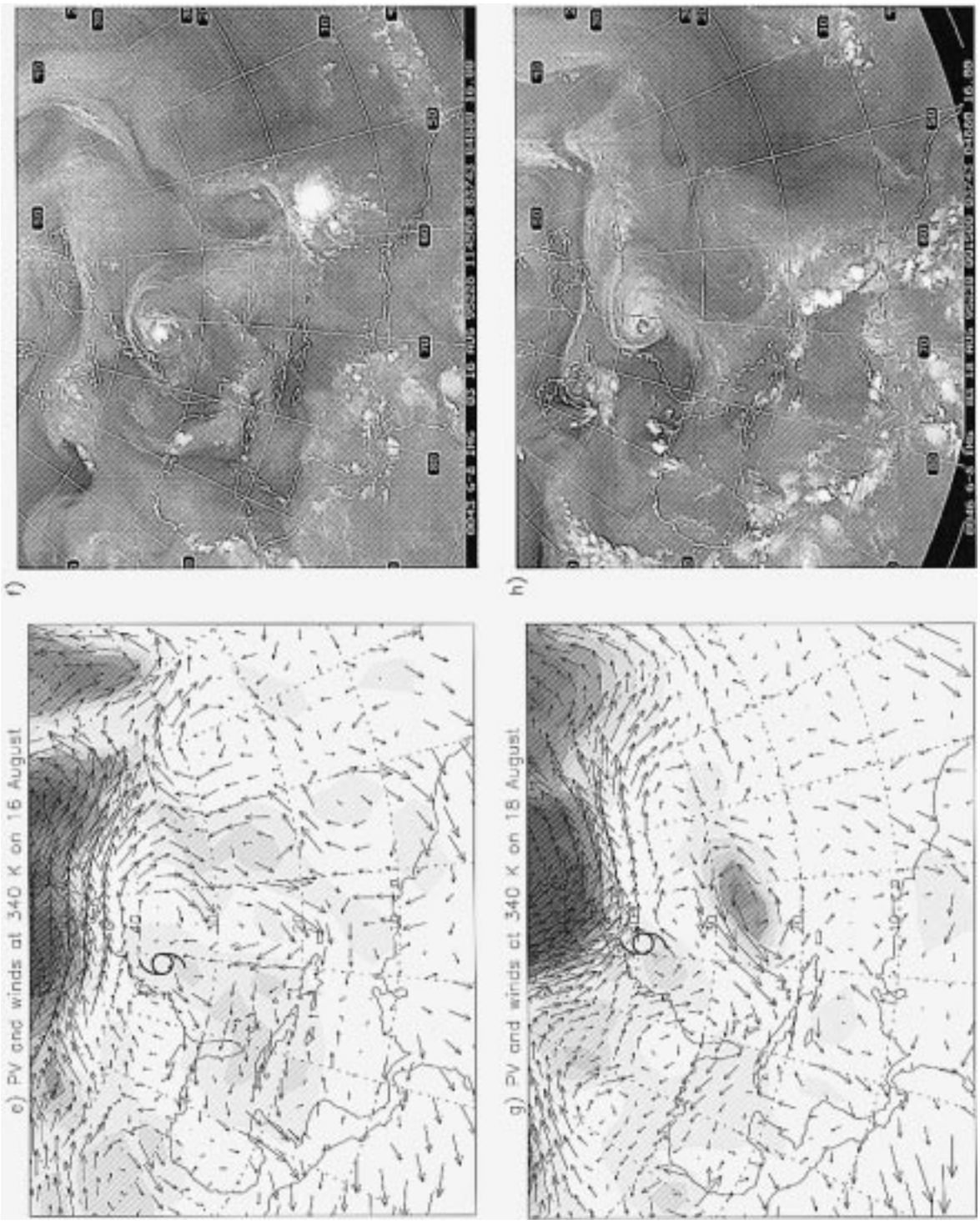

FIG. 1. (*Continued*) Lighter shading is used for PV values lower than 2 PVU and darker shading is used for PV values greater than 2 PVU. Contours are every 0.5 PVU where PV is lower than 2 PVU and every 1 PVU for regions where PV is greater than 2 PVU. A 5° long wind vector represents winds of 75 m s^{-1}.

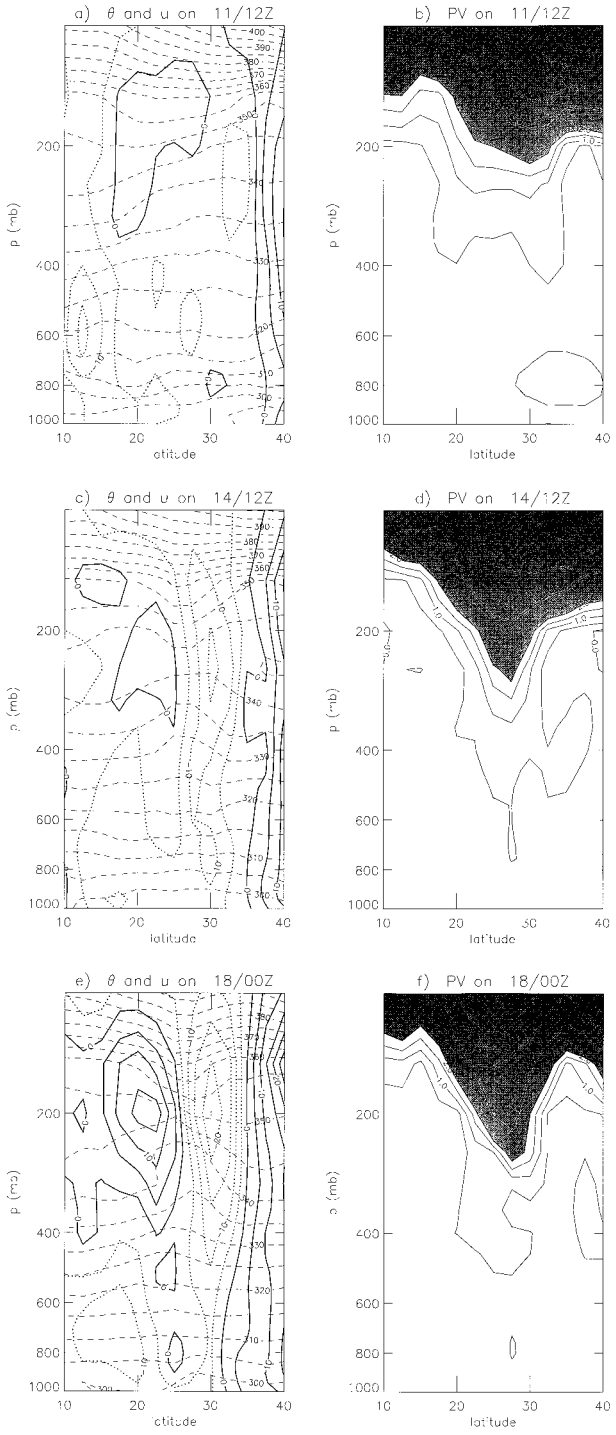

FIG. 2. Vertical cross sections of PV (PVU), zonal wind [m s^{-1}; thick lines in (a), (c), (e)] and potential temperature [K; thin dashed lines in (a), (c), (e)] showing the vertical structure of the TUTT cell: (a), (b) 11 Aug 1200 UTC at 30°W; (c), (d) 14 Aug 1200 UTC at 47.5°W; and (e), (f) 18 Aug 0000 UTC at 60°W.

$$\frac{\partial u}{\partial t} - hPv + \frac{\partial}{a\cos\phi\partial\lambda}\left[gh + \frac{1}{2}(u^2 + v^2)\right] = 0, \quad (1)$$

$$\frac{\partial v}{\partial t} + hPu + \frac{\partial}{a\partial\phi}\left[gh + \frac{1}{2}(u^2 + v^2)\right] = 0, \quad (2)$$

$$\frac{\partial h}{\partial t} + \frac{\partial(hu)}{a\cos\phi\partial\lambda} + \frac{\partial(hv\cos\phi)}{a\cos\phi\partial\phi} = 0, \quad (3)$$

where h is the fluid depth, a is the radius of the earth, $P = \zeta/h$ is the potential vorticity, and $\zeta = 2\Omega\sin\phi + \partial v/a\cos\phi\,\partial\lambda - \partial(u\cos\phi)/a\cos\phi\,\partial\phi$ is the absolute vorticity. We can regard (1)–(3) as a closed system in u, v, and h. For the simulations shown here, the mean initial fluid depth was 4500 m, which implies a gravity wave phase speed of 210 m s^{-1} and an equatorial Rossby length, $[a(\overline{gh})^{1/2}/(2\Omega)]^{1/2}$, of 3000 km. Spectral blocking (i.e., accumulation of enstrophy in the smallest resolved scales) is controlled by adding hyperdiffusion terms to the right-hand side of (1)–(3) (Jakob-Chien et al. 1995). The damping rates introduced by hyperdiffusion are small enough that it is probably useful to view the flow simulations as essentially conservative.

The numerical details of the global nonlinear shallow water model are given in Hack and Jakob (1992) and Jakob-Chien et al. (1995). It suffices here to say that the model's horizontal representation is based on spherical harmonics and triangular truncation with a maximum total wavenumber $N = 213$ is used in the simulations shown in this study.[3]

In the model, the circulation associated with a tropical cyclone is simulated by an imposed small circular patch of cyclonic vorticity centered near the equator (for convenience, this patch of cyclonic vorticity will be hereafter referred to as the *model tropical cyclone*). Likewise, the circumpolar vortex is simulated by an imposed large region of cyclonic vorticity centered at the pole (hereafter referred to as the *circumpolar cyclone*).

Initialization of the global shallow water model requires computation of the initial wind and mass fields associated with these vorticity patches. In order to compute the nondivergent wind field associated with these imposed vorticity distributions, the streamfunction ψ is obtained from the vorticity using

$$\nabla^2\psi = \zeta - 2\Omega\mu. \quad (4)$$

The winds are then computed from

$$u = -\frac{\partial\psi}{a\partial\phi} \quad \text{and} \quad v = \frac{\partial\psi}{a\cos\phi\partial\lambda}. \quad (5)$$

[3] Regarding the model's horizontal resolution, with a T213 truncation the number of real degrees of freedom for each dependent variable is $(214)^2$. If an equal area of the surface of the earth is associated with each real degree of freedom, this area equals $4\pi a^2/(214)^2 \approx 11\,134$ km^2. The square root of this area is approximately 106 km and is a useful estimate of the horizontal resolution of the T213 spherical harmonic spectral model (for further discussion, see Laprise 1992).

Finally, in order that transient gravity waves are kept to a minimum, the nonlinear balance equation is used to calculate the corresponding balanced mass field

$$g\nabla^2 h = \frac{\partial(v\zeta)}{a\cos\phi\partial\lambda} - \frac{\partial(u\zeta\cos\phi)}{a\cos\phi\partial\phi} - \nabla^2\left(\frac{u^2 + v^2}{2}\right). \quad (6)$$

Three types of initial value simulations were performed using the global nonlinear shallow water model. The first type of simulation shows the evolution of five model tropical cyclones that were initially placed in an environment at rest. The second type of simulation shows the interaction of the same five model tropical cyclones with a zonally symmetric circumpolar cyclone. Finally, the interaction of an asymmetric circumpolar cyclone with five model tropical cyclones is studied. In the asymmetric circumpolar cyclone simulations, inclusion of five model tropical cyclones has the advantage of allowing the study of five different evolutions in the same experiment. For consistency, all of the simulations presented here have five model tropical cyclones. The flow associated with each model tropical cyclone evolved almost independently from the others. This was determined by repeating one of the simulations with only one model tropical cyclone (not shown). Both the flow associated with this model tropical cyclone and its trajectory were nearly unchanged in the absence of the other four model tropical cyclones. Moreover, the use of five model tropical cyclones in our simulations is not unrealistic because during the most active months of the Northern Hemisphere's tropical cyclone season the simultaneous occurrence of several tropical cyclones around the globe is not uncommon. For instance, during the last week of August 1995, there were at least six tropical cyclones on any given day in the Atlantic and Pacific Oceans.

a. Model tropical cyclone in an environment at rest

The evolution of the wind and PV fields for the simulation that was initialized with five model tropical cyclones embedded in an environment at rest (hereafter referred to as MTC/ONLY) is shown in Fig. 3. Note that although the model's domain is the entire sphere, only the results for the Northern Hemisphere are displayed. Each model tropical cyclone has initial 2° radius and constant relative vorticity of 2×10^{-4} s^{-1}. The azimuthal winds were forced to vanish at 10° radius by adding anticyclonic vorticity in an annular region of 8° width around the model tropical cyclone. Radial profiles of vorticity as well as the corresponding balanced tangential winds for these model tropical cyclones are shown in Fig. 4. The tangential winds of our idealized cyclone are comparable to the midlevel tangential winds of tropical cyclones (Gray 1979).

The five model tropical cyclones were initially centered at 10°N and 72° apart (Fig. 3a). This simulation displays wavenumber-five symmetry, and therefore the forthcoming discussion of the flow produced by the model tropical cyclone that was initially placed at 0° longitude (hereafter referred to as MTC1) applies to all model tropical cyclones in this simulation. At five days (Fig. 3b), dispersion of short Rossby wave energy (Hoskins et al. 1977) is producing a wave train to the southeast of MTC1. At this time, the PV contours just to the east of MTC1 are undulating nearly reversibly due to the Rossby wave restoring mechanism predicted in linear Rossby wave theory. Approximately 1500 km southeast of MTC1 is a tropical trough that is the largest amplitude part of the Rossby wave train extending southeastward. This tropical trough has intensified with time and at day five there are northerlies of 6 m s^{-1} and southerlies of 3 m s^{-1} to its west and east, respectively. The axis of the tropical trough is oriented in the north-northeast–south-southwest (NNW–SSE) direction north of about 15°N and in the NNE–SSW direction south of 15°N. At day 10 (Fig. 3c), the NNW–SSE-oriented portion of the tropical trough has entered a more nonlinear stage of development with its PV contours rolling up and becoming irreversibly deformed. Note how the tropical trough becomes broader with time. On the east edge of the tropical trough, the flow is parallel to the PV contours, and on the west edge, the flow is across the PV contours in the sense of producing a broadening trough[4] (Thorncroft et al. 1993). The second tropical trough of the Rossby wave train is now present approximately 3000 km to the southeast of MTC1. After 14 days (Fig. 3d), the broadening tropical trough has evolved into a secondary cyclone 15° to the east of MTC1. The second tropical trough farther to the east of MTC1 is about to enter the highly nonlinear phase of a ''cyclonic breaker,'' which involves the roll up of PV contours.

The model tropical cyclones moved northwestward in a trajectory dictated by β drift, advection by environmental steering flows, and the meridional relative vorticity gradient (see Fig. 8). Throughout their lifetime, the tropical troughs moved west-northwestward, each closely following the motion of its corresponding model tropical cyclone.

b. Model tropical cyclone and zonally symmetric circumpolar cyclone interaction

In this section, results from a simulation in which the five equidistant model tropical cyclones interact with a zonally symmetric circumpolar cyclone (MTC/SCC) are presented. The meridional profile of zonal winds for the circumpolar cyclone at $t = 0$ are shown in Fig. 5. This profile is representative of the Northern Hemisphere

[4] Thorncroft et al. (1993) explained the thinning of midlatitude troughs embedded in anticyclonic shear and the broadening of midlatitude troughs embedded in cyclonic or weak anticyclonic shear using simple PV dynamics arguments.

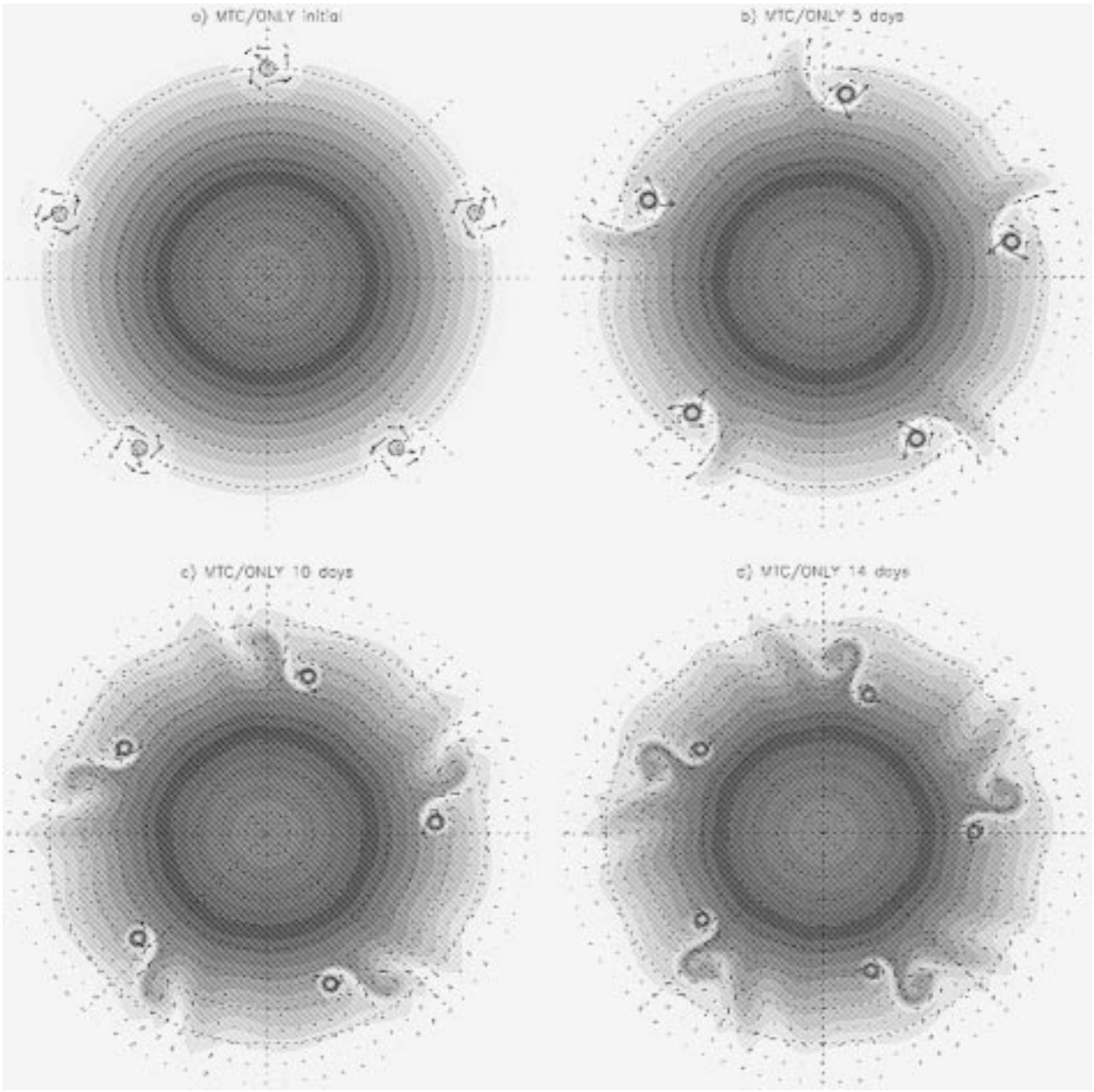

FIG. 3. The evolution of wind (m s^{-1}) and PV (s^{-1}) fields for the simulation that was initialized with five model tropical cyclones embedded in an environment at rest (MTC/ONLY); (a) initial, (b) 5 days, (c) 10 days, and (d) 14 days. Note the formation of broadening tropical troughs to the east of each model tropical cyclone.

zonally averaged summer tropospheric winds near 400 mb (Peixoto and Oort 1992). The circumpolar cyclone has maximum westerly winds of 10 m s^{-1} at 55°N. The zonal winds are easterly south of about 25°N with a maximum speed of 8 m s^{-1} at 5°N. This means that at the beginning of the simulation, the model tropical cyclones, which are centered at 10°N, are embedded in easterly winds and in an anticyclonic shear of about 3 $\times$ 10^{-6} s^{-1} (Fig. 6a).

A quite different evolution takes place in this case. After five days (Fig. 6b), dispersion of short Rossby wave energy has again begun to produce a wave train to the SE of MTC1. In this case, however, the tropical trough is being tilted in the NE–SW direction by the anticyclonic shear in which it is embedded. Note how the tropical trough becomes thinner and more elongated with time. This occurs because the flow is parallel to the PV contours on the east edge of the tropical trough and across the contours on the west edge, in the sense of producing a thinning trough (Thorncroft et al. 1993).

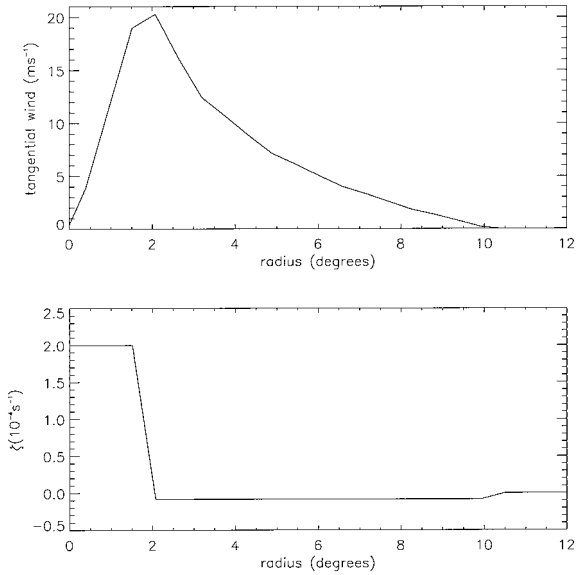

FIG. 4. Radial profiles of (a) tangential winds (m s^{-1}), and (b) relative vorticity for the model tropical cyclones used in our simulations.

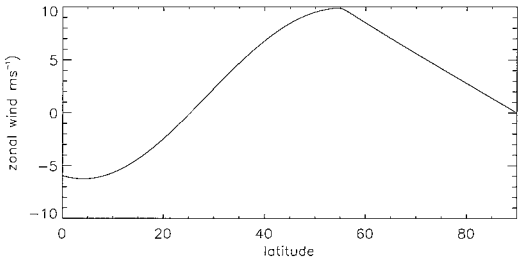

FIG. 5. Meridional profile of initial zonal wind (m s^{-1}) for the zonally symmetric circumpolar cyclone.

At 14 days (Fig. 6d), MTC1 has moved to 42°N and is about 35° to the east of its initial position. At that time the tropical trough is a thin and long filament of high PV that is tilted in the SW–NE direction and whose southwesternmost tip is begining to roll up. The signature of this thin filament of cyclonic PV in the fluid depth (not shown) and wind fields is nearly imperceptible. This is expected since inversion of the Laplacian operator in (4) has a smoothing effect that renders the fluid depth field nearly insensitive to small-scale features of the PV field. Some of the smoothing is passed on to the wind field following the differentiation in (5). Additional experiments showed that the transition between the ''broadening trough'' and ''thinning trough'' behaviors occurs gradually as the anticyclonic shear on the equatorward side of the circumpolar cyclone is increased.

The model tropical cyclones in MTC/SCC moved northwestward for about four days and then recurved and moved northeastward once they became embedded in the circumpolar cyclone's westerlies (see tracks in Fig. 8). The model tropical cyclones in MTC/SCC have moved about 14° farther northward than those in MTC/ONLY. The circumpolar vortex increases the northward gradient of absolute vorticity, enhancing the β effect and making the model tropical cyclones move farther north. The model tropical cyclones in MTC/SCC have also moved northeastward, steered by the mean westerly flow in which they were embedded, in contrast with the northwestward movement of those in MTC/ONLY.

Additional experiments in which a ring of anticyclonic winds was added around the model tropical cyclones (outside 10° radius) showed slower development of the tropical troughs to the east of the model tropical cyclones. This may occur because in these experiments the tropical troughs are embedded in the anticyclonic shear of the ring of anticyclonic winds. The model tropical cyclones were more efficient at producing tropical troughs in the absence of anticyclonic winds at large radii. In these experiments, southward advection of high-PV air to the east of the model tropical cyclones by the anticyclonic winds at large radii did not help intensify the tropical troughs.

It is also important to point out that the results shown in this section indicate that as one moves up in the troposphere, the increased intensity of the circumpolar vortex and decreased intensity of the tropical cyclone would tend to favor the thinning trough behavior.

c. Model tropical cyclone and asymmetric circumpolar cyclone interaction

The simulation presented in this section shows the interaction of the five model tropical cyclones with an asymmetric circumpolar cyclone (MTC/ACC). The circumpolar cyclone undulates with a wavenumber-six pattern (Figs. 7a,b) and its zonally averaged meridional profiles of absolute vorticity and zonal winds are the same as those for the circumpolar cyclone in MTC/SCC (Fig. 5). Wavenumber six was chosen because it is the typical wavelength of the most unstable baroclinic mode associated with the midlatitude jet. Due to the differences in position of each model tropical cyclone in relation to the nearby midlatitude waves, this simulation does not display wavenumber-five symmetry and the flow around each model tropical cyclone evolves differently. Interesting differences occurred in the mode of tropical trough formation (thinning vs broadening troughs) and in the trajectories followed by the model tropical cyclones. The evolution of two model tropical cyclones that are at opposite ends of the variability spectrum will be discussed, namely, the model tropical cyclones that were initially centered at 10°N, 72°W (MTC2), and 10°N, 72°E (MTC5).

The waves in the circumpolar cyclone moved eastward (with respect to the earth) north of 40°N and westward in lower latitudes. Their behavior also varies with latitude, with broadening troughs in the cyclonically sheared side of the jet (north of 55°N) and thinning

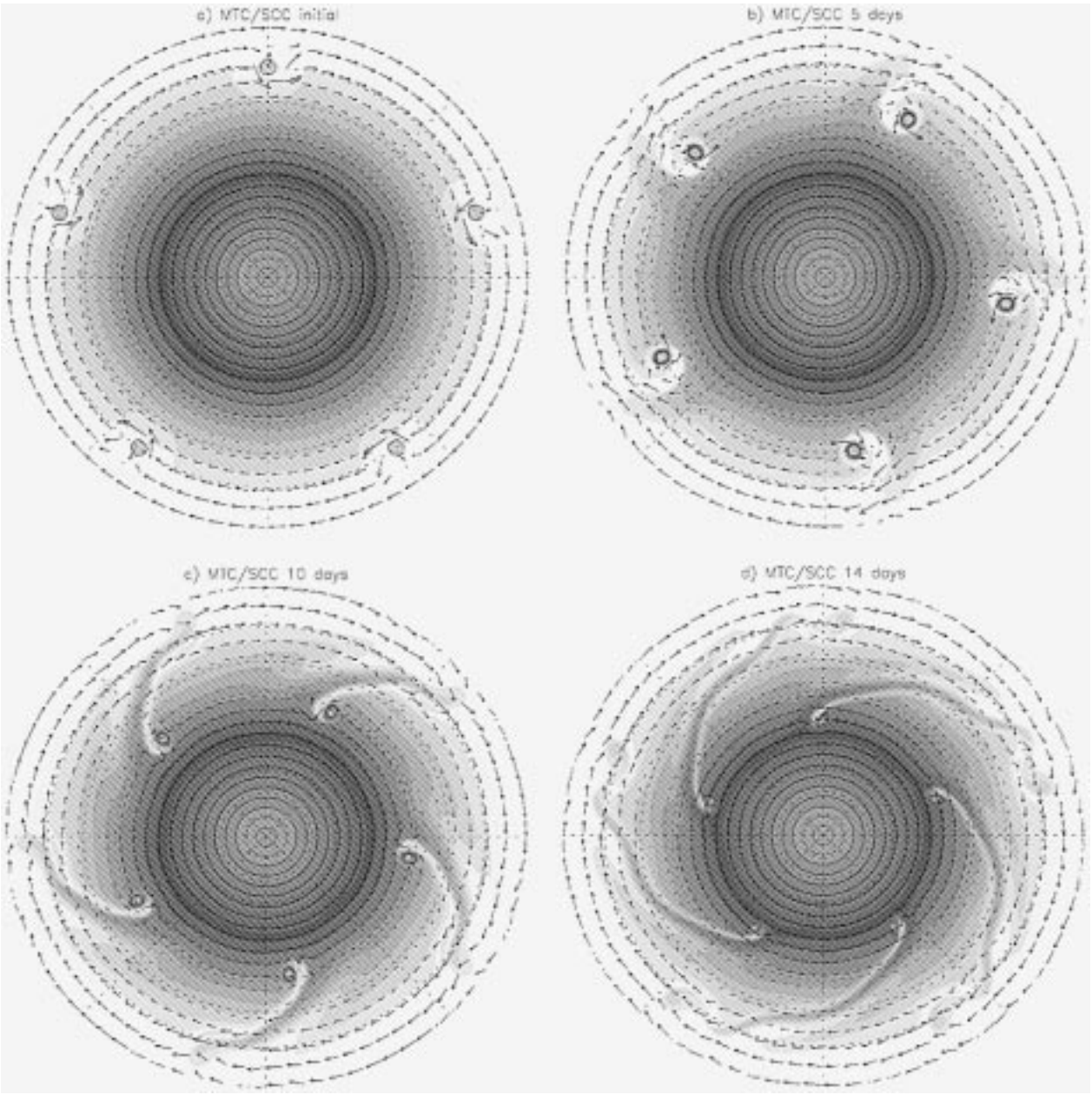

FIG. 6. Evolution of the wind (m s^{-1}) and PV (s^{-1}) fields for the simulation that was initialized with five model tropical cyclones and a zonally symmetric circumpolar vortex (MTC/SCC); (a) initial, (b) 5 days, (c) 10 days, and (d) 14 days. Note the formation of thinning tropical troughs to the east of each model tropical cyclone.

troughs in the anticyclonically sheared side of the jet (south of 55°N). Nakamura and Plumb (1994) attributed these asymmetries to differences in the location of critical layers around the westerly jet.

Figure 7 shows the evolution of the PV fields for this simulation. At $t = 0$ (Fig. 7a), MTC2 was located 12° to the west of a trough in the midlatitudes (hereafter referred to as T6). Downstream of T6, the other five troughs in the midlatitudes are named T2–T5. In the first few days, Rossby wave dispersion produces a tropical trough to the east of MTC2. At day 5 (Fig. 7b), this tropical trough is enhanced by the passage of T6 to its north. Note also that the tropical trough is becoming thin and tilted in the NE–SW direction. After 10 days (Fig. 7c), this tropical trough has become a long and thin undulating filament of high PV extending into the Tropics. The trajectories of the five model tropical cyclones are shown in Fig. 8. MTC2 follows an arc-shaped trajectory that has strong curvature, propagating northwestward for four days, then recurving near 25°N,

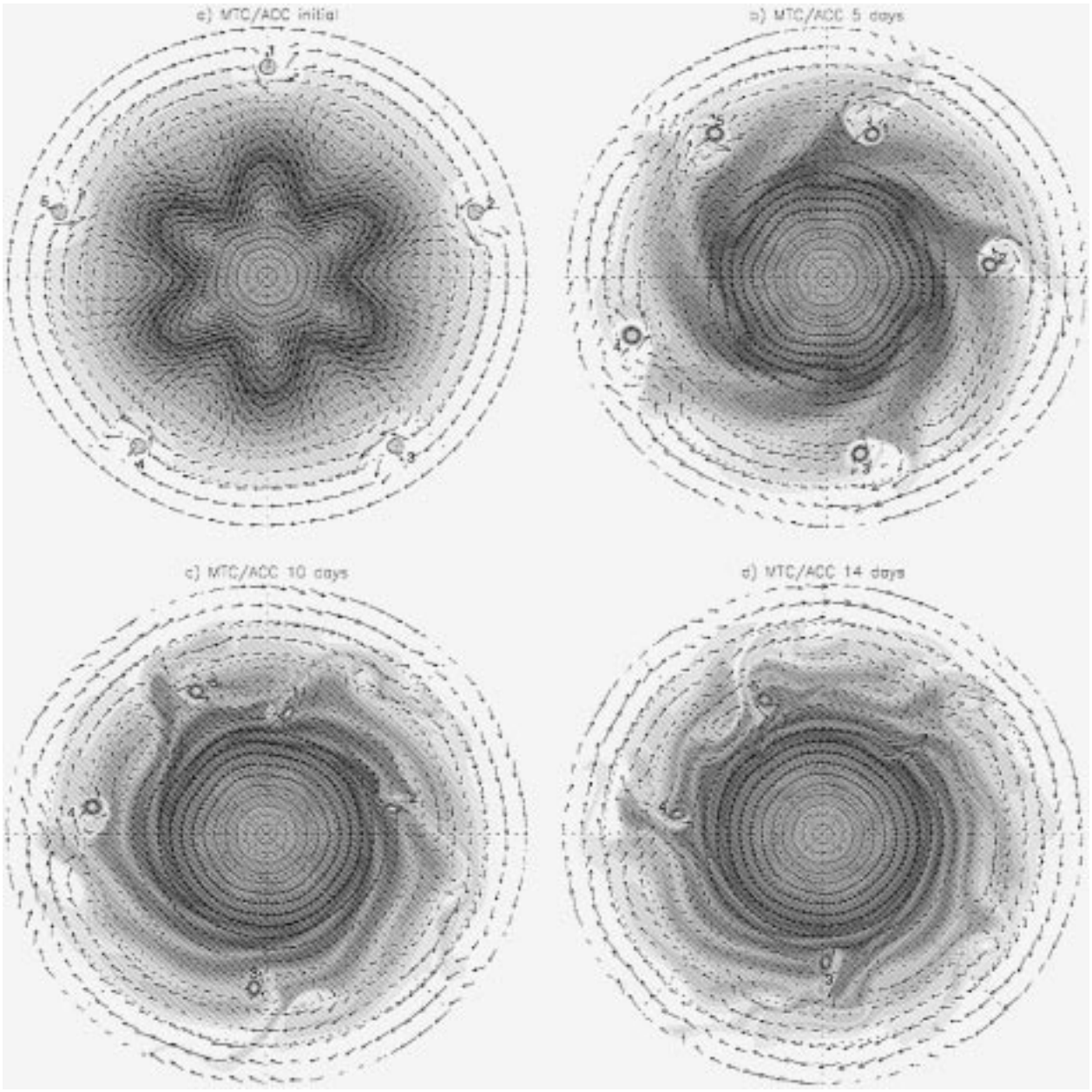

FIG. 7. Evolution of the wind (m s^{-1}) and PV (s^{-1}) fields for the simulation that was initialized with five model tropical cyclones and an asymmetric circumpolar vortex (MTC/ACC); (a) initial, (b) 5 days, (c) 10 days, and (d) 14 days.

getting caught in the westerlies at day 10, and propagating eastward thereafter.

At $t = 0$ (Fig. 7a), MTC5 was located 12° to the east of a trough in the midlatitudes (T2). In a few days, Rossby wave dispersion produced a tropical trough to the east of MTC5 (Fig. 7b). After a couple of days, MTC5's tropical trough has been enhanced by interaction with T4. In this case, however, the tropical trough to the east of the model tropical cyclone displays the broadening behavior. By day 10 (Fig. 7c) the broad tropical trough is being enhanced by interaction with T2. Note the strong meridional winds (in excess of 8 m s^{-1}) around MTC5's tropical trough. The trajectories of MTC2 and MTC5 are very different (Fig. 8): while MTC2 moved initially northwestward and then recurved, MTC5 followed a long west-northwestward trajectory without recurving during the simulation. The tropical trough to the east of MTC5 followed a long westward trajectory accompanying MTC5.

Regarding the remaining model tropical cyclones, MTC1 and MTC3 produced thinning tropical troughs, and MTC4 produced a broadening tropical trough. Note

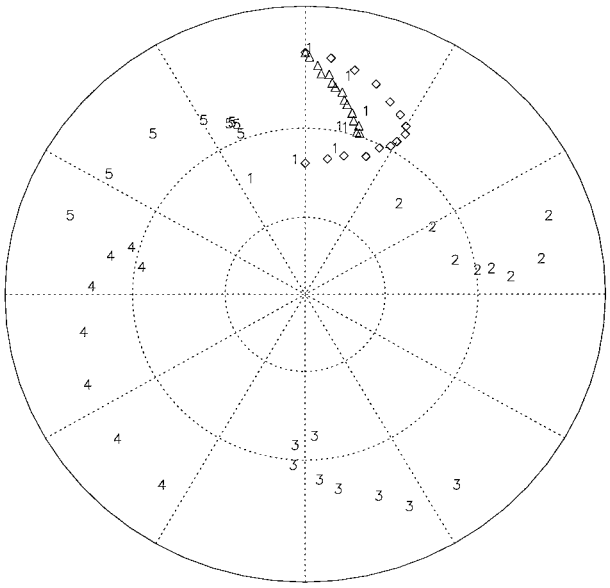

FIG. 8. Trajectories of the five model tropical cyclones in MTC/ONLY (pluses), MTC/SCC (squares), and MTC/ACC (triangles). Marks along each 15-day trajectory are 1 day apart. Only one trajectory is shown for MTC/ONLY and MTC/SCC because of the five-fold symmetry in these simulations.

how, to various degrees, the thinning tropical troughs in this simulation tend to undulate and break down through barotropic instability. There is a reversal in the PV gradient across the thinning tropical troughs that renders them barotropically unstable. The instability and breakdown of the thinning tropical troughs occurs despite the stabilizing influence of the flow field of the circumpolar vortex. Dritschel (1989) found that, in the presence of sufficient adverse shear, such as the anticyclonic shear to the south of the circumpolar vortex, PV filaments can become stable and undulation and breakdown are prevented. The trajectories of MTC1, MTC3, and MTC4 fall somewhere between the more or less straight westward trajectory followed by MTC1 and the recurving trajectory followed by MTC5 (Fig. 8).

A phase difference of only 12° between the initial positions of MTC1 and MTC2 with respect to the troughs in the midlatitudes was responsible for a large difference in the trajectories they followed and in the mode of evolution of the tropical troughs to their east. Namely, while MTC1 produced a thinning trough that had very small effect upon the fluid depth (not shown) and PV fields, MTC2 produced a broadening trough that was accompanied by a strong signature in the fluid depth (not shown) and wind fields. This suggests that the mode of formation of TUTTs by tropical cyclones may be strongly dependent upon interactions with midlatitude waves. The broadening tropical trough formed by MTC2 bears resemblance with the TUTT that formed in the wake of Hurricane Felix.

4. Wave–mean flow interaction

If one studies sequences of satellite images such as the one shown in Fig. 1, an impression of intense dynamic activity in the upper troposphere emerges. What effect does such dynamic activity have on the zonal mean circulation? This question can be addressed using the shallow water version of wave–mean flow theory that is now reviewed.

a. Derivation of the zonal mean equations

The zonal mean equations can be used to study the influence of a tropical cyclone upon the zonal mean circulation in which it is embedded. To derive the zonal mean equations from (1)–(3) two types of zonal average are defined: an ordinary zonal average and a mass-weighted zonal average. For example, for the zonal wind u, the ordinary zonal average is defined by

$$\overline{u}(\phi, t) = \frac{1}{2\pi}\int_0^{2\pi} u(\lambda, \phi, t)\, d\lambda. \tag{7}$$

For the meridional wind v, the mass-weighted zonal average is defined by

$$\hat{v} = \frac{\overline{hv}}{\overline{h}}. \tag{8}$$

Deviations from the ordinary zonal average of u are defined by $u' = u - \overline{u}$ and deviations from the mass-weighted zonal average of v by $v^* = v - \hat{v}$. Similar definitions hold for the other variables.

Applying $\overline{(\,)}$ to each term in (3) and noting from (8) that $\overline{hv} = \overline{h}\hat{v}$, we can write the zonal mean mass continuity equation as

$$\frac{\partial \overline{h}}{\partial t} + \frac{\partial(\overline{h}\hat{v}\cos\phi)}{a\cos\phi\partial\phi} = 0. \tag{9}$$

This equation can also be written in the advective form (16).

To derive the equation for the mean zonal motion we first apply the $\overline{(\,)}$ operator to each term in (1), which yields

$$\frac{\partial \overline{u}}{\partial t} - \overline{hPv} = 0. \tag{10}$$

Noting that $P = \hat{P} + P^*$ and $v = \hat{v} + v^*$, we can write $\overline{hPv} = \overline{h}\hat{P}\hat{v} + \overline{hP^*v^*}$ since $\overline{hv^*} = 0$ and $\overline{hP^*} = 0$. Thus, (10) can be written as

$$\frac{\partial \overline{u}}{\partial t} - \overline{h}\hat{P}\hat{v} = \mathcal{F}, \tag{11}$$

where $\mathcal{F}$ is defined below in (18). Noting that $a\mathcal{D}\phi/\mathcal{D}t = \hat{v}$ [easily confirmed by applying (17) to ϕ] and that $\overline{h}\hat{P} = \overline{\zeta} = 2\Omega\sin\phi - \partial(\overline{u}\cos\phi)/(a\cos\phi\,\partial\phi)$, (11) can be written in the absolute angular momentum form given below in (14).

Now consider the meridional momentum equation.

Since both (16) and (17) contain $\hat{v}$, we would like to transform (2) into a prediction equation for $\hat{v}$. This requires putting (2) into a flux form before taking the zonal average. Thus, combining (2) and (3), we obtain the flux form:

$$\frac{\partial(hv)}{\partial t} + \frac{\partial(huv)}{a\cos\phi\partial\lambda} + \frac{\partial(hvv\cos\phi)}{a\cos\phi\partial\phi} + \left(2\Omega\sin\phi + \frac{u\tan\phi}{a}\right)hu + gh\frac{\partial h}{a\partial\phi} = 0. \quad (12)$$

Taking the zonal average of (12), we obtain

$$\frac{\partial(\overline{hv})}{\partial t} + \frac{\partial(\overline{hvv}\cos\phi)}{a\cos\phi\partial\phi} + \overline{\left(2\Omega\sin\phi + \frac{u\tan\phi}{a}\right)hu} + gh\overline{\frac{\partial h}{a\partial\phi}} = 0. \quad (13)$$

Noting that $\overline{hv} = \overline{h}\hat{v}$, $\overline{hvv} = \overline{h}\hat{v}\hat{v} + \overline{hv^*v^*}$, $\overline{h\,\partial h/(a\partial\phi)} = \overline{h}\,\partial\overline{h}/(a\,\partial\phi) + \overline{h'\,\partial h'/(a\,\partial\phi)}$, and using the zonal mean continuity equation [(9)], we obtain the advective form (15).

Collecting the above results we obtain the complete set of zonal mean flow equations:

$$\frac{\mathcal{D}(\overline{u}\cos\phi + \Omega a\cos^2\phi)}{\mathcal{D}t} = \mathcal{F}\cos\phi, \quad (14)$$

$$\frac{\mathcal{D}\hat{v}}{\mathcal{D}t} + \left(2\Omega\sin\phi + \frac{\overline{u}\tan\phi}{a}\right)\overline{u} + g\frac{\partial\overline{h}}{a\partial\phi} = \mathcal{G}, \quad (15)$$

$$\frac{\mathcal{D}\overline{h}}{\mathcal{D}t} + \overline{h}\frac{\partial(\hat{v}\cos\phi)}{a\cos\phi\partial\phi} = 0, \quad (16)$$

where

$$\frac{\mathcal{D}}{\mathcal{D}t} = \frac{\partial}{\partial t} + \hat{v}\frac{\partial}{a\partial\phi} \quad (17)$$

is the derivative following the mass-weighted mean meridional circulation and

$$\mathcal{F} = \overline{hP^*v^*} = -\frac{1}{\overline{h}}\left\{\frac{\partial[\overline{(hv)'u'}\cos^2\phi]}{a\cos^2\phi\partial\phi} + \frac{\partial[\overline{h'u'}]}{\partial t}\right\} \quad (18)$$

$$\mathcal{G} = -\frac{1}{\overline{h}}\left[\frac{\partial(\overline{hv^*v^*}\cos\phi)}{a\cos\phi\partial\phi} + \left(2\Omega\sin\phi + \frac{\overline{u}\tan\phi}{a}\right)\overline{h'u'} + \frac{\overline{(hu)'u'}\tan\phi}{a} + \overline{h'\frac{\partial h'}{a\partial\phi}}\right] \quad (19)$$

are the eddy-induced effective mean zonal and meridional forces per unit mass. Equations (14)–(16) have the form of the zonally symmetric primitive equations for $\overline{u}$, $\hat{v}$, and $\overline{h}$, all of which are functions of (ϕ, t). The terms $\mathcal{F}$ and $\mathcal{G}$ appear as forcings. As discussed by Andrews (1983), Tung (1986), and in the appendix here, it is also possible to express $\mathcal{F}$ in the form given by the second half of (18). This form involves the divergence (or, more properly, pseudodivergence) of the Eliassen–Palm flux. This relation is helpful in understanding how zonal asymmetries can influence the mean zonal flow by producing a meridional eddy flux of PV or, equivalently, a pseudodivergence of the Eliassen–Palm flux.

Section 4b focuses on understanding the interactions of symmetric and asymmetric components of the flow and, in particular, the influence of tropical cyclones on the zonal mean circulation.

b. Results

Figure 9 shows meridional profiles of $\overline{P}$, $\overline{hP^*v^*}$, and the change in $\overline{u}$ ($\Delta\overline{u}$) during the three simulations discussed in section 3 and a fourth simulation that was initialized with the asymmetric circumpolar cyclone alone (ACC/ONLY).

The signature of the model tropical cyclones in the meridional profile of $\overline{P}$ is a region of increased PV near 10°N that is about 6° wide at day 1 (Figs. 9a,c,e). In MTC/ONLY, the signature of the model tropical cyclones is displaced to 30°N after 14 days. During MTC/ONLY, the meridional gradient of $\overline{P}$ between 15°N and 28°N decreased as a consequence of wave breaking during the formation of the broad tropical troughs in Fig. 3d. Such regions of decreased meridional PV gradient are called *surf zones*, denoting the occurrence of wave breaking with PV contours rolling up and becoming irreversibly deformed (McIntyre and Palmer 1984). Episodes of wave breaking in which PV contours roll up as in MTC/ONLY are efficient in mixing PV and producing a surf zone. Note how, during the formation of the thinning troughs in MTC/SCC, wave breaking was not efficient in producing a wide surf zone (Fig. 9c). Instead, two thin regions of decreased PV gradient centered near 10°N and 20°N were produced by the undulations in the thinning tropical trough seen in Fig. 6d.

The time-integrated meridional eddy fluxes of PV for MTC/ONLY and MTC/SCC at 1 and 15 days are shown in Figs. 9b,d. The model tropical cyclones produce a southward–northward–southward pattern of meridional eddy fluxes of PV, which is clearly seen centered near 10°N in day 1 (dashed lines in Figs. 9b,d). As the model tropical cyclones move northward, they produce a northward eddy flux of PV that, according to Eq. (14), is associated with a westerly acceleration of the mean zonal flow. On the southern and northern flanks of the model tropical cyclones, southward eddy fluxes of PV and an easterly acceleration of the zonal mean flow prevail as the model tropical cyclones wrap PV contours around themselves. After 15 days, the net effect of the model tropical cyclones in MTC/ONLY and MTC/SCC upon the mean zonal flow has been to produce alternating regions of easterly and westerly acceleration. Easterly acceleration of the mean zonal flow, with peaks of up to 1 m s^{-1} per 15 days, dominated south of 10°N and north of the northernmost position of the model tropical cyclones. Westerly acceleration of the mean zonal flow,

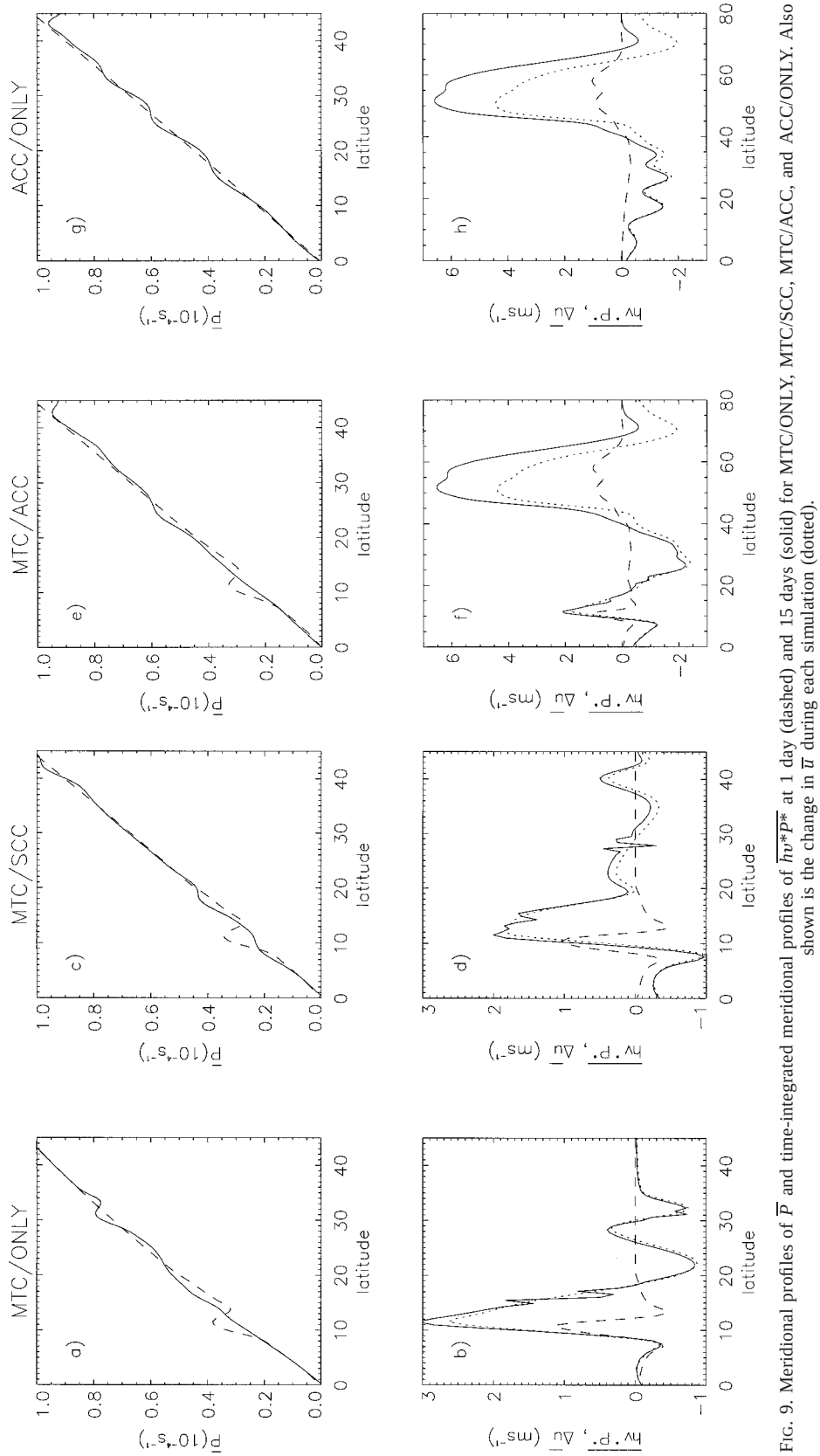

FIG. 9. Meridional profiles of $\overline{P}$ and time-integrated meridional profiles of $\overline{hv^*P^*}$ at 1 day (dashed) and 15 days (solid) for MTC/ONLY, MTC/SCC, MTC/ACC, and ACC/ONLY. Also shown is the change in $\overline{u}$ during each simulation (dotted).

with peaks of up to 3 m s^{-1} per 15 days, dominated in the latitudinal belt through which the model tropical cyclones traveled. The dotted lines in Figs. 9b,d show the change in $\overline{u}$ during MTC/ONLY and MTC/SCC. There is good agreement between the change in $\overline{u}$ during the simulation and the time-integrated eddy-induced effective mean zonal forcing calculated using wave–mean flow theory. The discrepancies between these two terms are accounted for by the $\overline{h}\hat{P}\hat{v}$ term in Eq. (11), which increases with latitude and also with the higher $\hat{v}$ of the simulations that include a circumpolar vortex.

In the simulation that was initialized with the asymmetric circumpolar vortex alone (ACC/ONLY), breaking of the midlatitude barotropic waves produced eastward acceleration of the mean zonal flow (with peaks of up to 6 m s^{-1} per 15 days) between 40° and 65°N, and westward acceleration elsewhere (with peaks around -2 m s^{-1} per 15 days). This pattern of mean zonal flow changes is in good agreement with the results of Held and Phillips (1987, 1990). In simulations of the barotropic decay of midlatitude waves, Held and Phillips (1987) found an acceleration of the mean westerly zonal flow in the region of wave excitation (where the midlatitude waves have maximum initial amplitude) and deceleration in two surrouding latitudinal bands (critical layers) where wave absorption occurs. During MTC/ACC and ACC/ONLY the edge of the circumpolar cyclone is sharpened as evidenced by the increase in the meridional gradient of $\overline{P}$ between 45° and 65°N (Figs. 9e,g). This sharpening of the edge of the circumpolar cyclone occurs as the circumpolar cyclone axisymmetrizes through ejection of high-PV filaments (e.g., Melander et al. 1987; Juckes and McIntyre 1987; Polvani and Plumb 1992). In addition to the changes in zonal wind caused by the decay of the midlatitude waves, the model tropical cyclones in MTC/ACC cause an eastward acceleration of the mean zonal flow between 10° and 20°N analogous to the one discussed in MTC/ONLY and MTC/SCC. In MTC/ACC and ACC/ONLY, the agreement between the change in $\overline{u}$ and the eddy-induced effective mean zonal forcing calculated using wave–mean flow theory deteriorates away from the equator.

5. Concluding remarks

The interaction of tropical cyclones with their environment was studied within the idealized framework of a global nonlinear shallow water model. Dispersion of short Rossby wave energy and the formation of a wave train to the east of cyclones or anticyclones are intrinsic properties of flow on a rotating sphere.[5]

Based on the results of the shallow water simulations, and keeping in mind their limitations, we propose that dispersion of short Rossby wave energy is a possible mechanism to explain the formation of TUTT cells to the east of tropical cyclones. The model simulations suggest that two types of TUTT cell may form to the east of tropical cyclones. In the presence of cyclonic or weak anticyclonic shear, the trough to the east of the tropical cyclone may broaden, resulting in the formation of an intense TUTT cell that has a strong signature in the wind and mass fields. When the anticyclonic shear exceeds a certain threshold, the trough to the east of the tropical cyclone may become a thin and elongated TUTT cell that has comparatively negligible signature in the mass and flow fields. In the model, undulation and breakdown of thinning tropical troughs was common. The model simulations indicate that the mode of evolution of TUTT cells that form to the east of a tropical cyclone is strongly dependent on the intensity and relative location of midlatitude waves. Our results also indicate that as one moves up in the troposphere, the increased intensity of the circumpolar vortex and decreased intensity of the tropical cyclone would tend to favor the thinning trough behavior.

Possible effects of tropical cyclones upon the mean zonal flow were also assessed within the framework of the shallow water model. The model tropical cyclones produced a westerly acceleration of the mean zonal flow in the latitudinal band through which they moved and an easterly acceleration elsewhere.

Regarding the influence of TUTT cells upon the mean zonal flow, potential vorticity rearrangement due to TUTT cells would appear to result in a southward eddy flux of PV, that is, $\mathcal{F} = \overline{hP^*v^*} < 0$. A southward eddy flux of PV and corresponding westward acceleration of the zonal mean flow are caused by the broadening trough studied in section 3b. No direct effect of thinning troughs on the acceleration of the mean flow can be inferred from the results shown in section 3c. Yet an interesting question is whether the eddy-induced effective mean zonal force per unit mass $\overline{hP^*v^*}$ can ever be of such a large magnitude that it plays as important a role as diabatic heating in shaping the Hadley circulation.

As mentioned in the introduction, the main limitation of this study is imposed by the different vertical structures of the circumpolar vortex and tropical cyclones and the lack of diabatic effects. With the use of a shallow water model, we do not mean to imply that vertical stratification and diabatic effects are not important in the interaction of tropical cyclones with midlatitude waves. This is only a first step in understanding the complicated nonlinear interactions between tropical cyclones and the circumpolar vortex and it is clear that further work using a multilayer global model that includes diabatic effects is needed.

Acknowledgments. We thank James Hack for the use

[5] The strength of short Rossby wave energy dispersion is directly proportional to the relative angular momentum of the barotropic cyclone (e.g., Shapiro and Ooyama 1990). For instance, a barotropic vortex that has zero relative angular momentum has reduced far-field effects.

of his global nonlinear shallow water model and Raymond Zehr and John Knaff for providing the *GOES-8* water vapor images. We are also grateful to Lloyd Shapiro and two anonymous reviewers for their careful review of an earlier version of this paper. NCAR provided the ECMWF data. This work was supported by the National Science Foundation, under Grants ATM-9422525 and ATM-9729970, and by NOAA through TOGA COARE Grants NA37RJ0202 (item 16) and NA67RJ0152 (amendment 17). Rosana Nieto Ferreira was in part supported by USRA under Contract NAS5-32484.

APPENDIX

The Primitive Equation Form of the Taylor Relation

As discussed by Tung (1986), the primitive equation form of the Taylor relation can be obtained by deriving an alternate form of the absolute angular momentum principle, followed by a comparison with Eq. (14). The alternate derivation of the absolute angular momentum principle begins by writing the zonal wind equation [(1)] in the flux form:

$$\frac{\partial(hu)}{\partial t} + \frac{\partial(huu)}{a\cos\phi\partial\lambda} + \frac{\partial(huv\cos^2\phi)}{a\cos^2\phi\partial\phi} - 2\Omega\sin\phi hv + gh\frac{\partial h}{a\cos\phi\partial\lambda} = 0. \quad \text{(A1)}$$

Taking the zonal average of (A1) we obtain

$$\frac{\partial(\overline{hu})}{\partial t} + \frac{\partial(\overline{huv}\cos^2\phi)}{a\cos^2\phi\partial\phi} - 2\Omega\sin\phi\overline{hv} = 0. \quad \text{(A2)}$$

Noting that $\overline{hv} = \overline{h}\hat{v}$, $\overline{hu} = \overline{h}\,\overline{u} + \overline{h'u'}$ we obtain

$$\frac{\mathcal{D}(\overline{u}\cos\phi + \Omega a\cos^2\phi)}{\mathcal{D}t} = -\frac{1}{\overline{h}}\left\{\frac{\partial[\overline{(hv)'u'}\cos^2\phi]}{a\cos\phi\partial\phi} + \frac{\partial[\overline{h'u'}\cos\phi]}{\partial t}\right\}, \quad \text{(A3)}$$

where $\mathcal{D}/\mathcal{D}t$ is defined by (17). Since the left-hand sides of Eqs. (14) and (A3) are identical, the right-hand sides of these two equations must be equal, which results in

$$\overline{hP^*v^*} = -\frac{1}{\overline{h}}\left\{\frac{\partial[\overline{(hv)'u'}\cos^2\phi]}{a\cos^2\phi\partial\phi} + \frac{\partial[\overline{h'u'}]}{\partial t}\right\}. \quad \text{(A4)}$$

This is the relation used in (18).

REFERENCES

Andrews, D. G., 1983: A finite amplitude Eliassen–Palm theorem in isentropic coordinates. *J. Atmos. Sci.,* **40,** 1877–1883.

Appenzeller, C., H. C. Davies, and W. A. Norton, 1996: Fragmentation of stratospheric intrusions. *J. Geophys. Res.,* **101,** 1435–1456.

Colton, D. E., 1973: Barotropic scale interactions in the tropical upper troposphere during the northern summer. *J. Atmos. Sci.,* **30,** 1287–1302.

Dritschel, D. G., 1989: On the stabilization of a two-dimensional vortex strip by adverse shear. *J. Fluid Mech.,* **206,** 193–221.

Gallimore, R. G., and D. R. Johnson, 1981: The forcing of the meridional circulation of the isentropic zonally averaged circumpolar vortex. *J. Atmos. Sci.,* **38,** 583–599.

Gray, W. M., 1968: Global view of the origin of tropical disturbances and storms. *Mon. Wea. Rev.,* **96,** 669–700.

——, 1979: Hurricanes: Their formation, structure and likely role in the tropical circulation. *Meteorology over the Tropical Oceans,* D. B. Shaw, Ed., Royal Meteorological Society, 155–218.

Habjan, E. E., and G. J. Holland, 1995: Extratropical transitions of tropical cyclones in the western Australia region. *Proc. 21st Conf. on Hurricanes and Tropical Meteorology,* Miami, FL, Amer. Meteor. Soc., 310–311.

Hack, J. J., and R. Jakob, 1992: Description of a global shallow water model based on the transform method. NCAR Tech. Note NCAR/TN-343+STR, 39 pp. [Available from Climate and Global Dynamics Divisions, NCAR, P.O. Box 3000, Boulder, CO 80307.]

Held, I., and P. J. Phillips, 1987: Linear and nonlinear barotropic decay on the sphere. *J. Atmos. Sci.,* **44,** 200–207.

——, and ——, 1990: A barotropic model of the interaction between the Hadley cell and a Rossby wave. *J. Atmos. Sci.,* **47,** 856–869.

Hodanish, S., and W. M. Gray, 1993: An observational analysis of tropical cyclone recurvature. *Mon. Wea. Rev.,* **121,** 2665–2689.

Holton, J. R., P. H. Haynes, M. E. McIntyre, A. R. Douglass, R. B. Rood, and L. Pfister, 1995: Stratosphere-troposphere exchange. *Rev. Geophys.,* **33,** 403–439.

Hoskins, B. J., and M. J. Rodwell, 1995: A model of the Asian summer monsoon. Part I: The global scale. *J. Atmos. Sci.,* **52,** 1329–1340.

——, A. J. Simmons, and D. G. Andrews, 1977: Energy dispersion in a barotropic atmosphere. *Quart. J. Roy. Meteor. Soc.,* **103,** 553–567.

——, M. E. McIntyre, and A. W. Robertson, 1985: On the use and significance of isentropic potential vorticity maps. *Quart. J. Roy. Meteor. Soc.,* **111,** 877–946.

Jakob-Chien, R. J., J. J. Hack, and D. L. Williamson, 1995: Spectral transform solutions to the shallow water test set. *J. Comput. Phys.,* **119,** 164–187.

Joly, A., and A. J. Thorpe, 1990: Frontal instability generated by tropospheric potential vorticity anomalies. *Quart. J. Roy. Meteor. Soc.,* **116,** 525–560.

Juckes, M. N., and M. E. McIntyre, 1987: A high-resolution one-layer model of breaking planetary waves in the stratosphere. *Nature,* **328,** 590–596.

Kelley, W. E., Jr., and D. R. Mock, 1982: A diagnostic study of upper tropospheric cold lows over the western North Pacific. *Mon. Wea. Rev.,* **110,** 471–480.

Laprise, R., 1992: The resolution of global spectral models. *Bull. Amer. Meteor. Soc.,* **73,** 1453–1454.

McIntyre, M. E., and T. N. Palmer, 1984: The ''surf zone'' in the stratosphere. *J. Atmos. Terr. Phys.,* **46,** 825–849.

Melander, M. V., J. C. McWilliams, and N. J. Zabusky, 1987: Axisymmetrization and vorticity-gradient intensification of an isolated two-dimensional vortex through filamentation. *J. Fluid Mech.,* **178,** 137–159.

Molinari, J., S. Skubis, and D. Vollaro, 1995: External influences on hurricane intensity. Part III: Potential vorticity structure. *J. Atmos. Sci.,* **52,** 3593–3606.

Montgomery, M. T., and B. F. Farrell, 1993: Tropical cyclone formation. *J. Atmos. Sci.,* **50,** 285–310.

Nakamura, M., and R. A. Plumb, 1994: The effects of flow asymmetry on the direction of Rossby wave breaking. *J. Atmos. Sci.,* **51,** 2031–2045.

Nieto Ferreira, R., and W. H. Schubert, 1997: Barotropic aspects of ITCZ breakdown. *J. Atmos. Sci.,* **54,** 261–285.

Peixoto, J. P., and A. H. Oort, 1992: *Physics of Climate*. American Institute of Physics, 520 pp.

Pfeffer, R. L., 1981: Wave-mean flow interactions in the atmosphere. *J. Atmos. Sci.,* **38,** 1340–1359.

——, and M. Challa, 1992: The role of environmental asymmetries in Atlantic hurricane formation. *J. Atmos. Sci.,* **49,** 1051–1059.

Polvani, L. M., and R. A. Plumb, 1992: Rossby wave breaking, microbreaking, filamentation, and secondary vortex formation: The dynamics of a perturbed vortex. *J. Atmos. Sci.,* **49,** 462–476.

Price, J. D., and G. Vaughan, 1992: Statistical studies of cut-off-low systems. *Ann. Geophys.,* **10,** 96–102.

——, and ——, 1993: The potential for stratosphere-troposphere exchange in cut-off-low systems. *Quart. J. Roy. Meteor. Soc.,* **119,** 343–365.

Sadler, J., 1975: The upper tropospheric circulation over the global tropics. UHMET 75-02, 103 pp. [Available from the Department of Meteorology, University of Hawaii at Manoa, 2525 Correa Rd., Honolulu, HI 96822.]

Shapiro, L. J., and K. V. Ooyama, 1990: Barotropic vortex evolution on a beta plane. *J. Atmos. Sci.,* **47,** 170–187.

Silva Dias, P. L., W. H. Schubert, and M. DeMaria, 1983: Large-scale response of the tropical atmosphere to transient convection. *J. Atmos. Sci.,* **40,** 2689–2707.

Thorncroft, C. D., B. J. Hoskins, and M. E. McIntyre, 1993: Two paradigms of baroclinic-wave life-cycle behaviour. *Quart. J. Roy. Meteor. Soc.,* **119,** 17–55.

Thorpe, A. J., 1985: Diagnosis of balanced vortex structure using potential vorticity. *J. Atmos. Sci.,* **42,** 397–406.

Tung, K. K., 1986: Nongeostrophic theory of zonally averaged circulation. Part I: Formulation. *J. Atmos. Sci.,* **43,** 2600–2618.

Webster, P. J., 1972: Response of the tropical atmosphere to local steady forcing. *Mon. Wea. Rev.,* **100,** 518–541.

Whitfield, M. B., and S. W. Lyons, 1992: An upper-level low over Texas during summer. *Wea. Forecasting,* **7,** 89–106.